ACS Catalysis

Research Article

Cite This: ACS Catal. 2019, 9, 10780−10793

pubs.acs.org/acscatalysis

Plasma-Enhanced Catalytic Synthesis of Ammonia over a Ni/Al_2O_3 Catalyst at Near-Room Temperature: Insights into the Importance of the Catalyst Surface on the Reaction Mechanism

Yaolin Wang,[†] Michael Craven,[†] Xiaotong Yu,[†] Jia Ding,[‡] Paul Bryant,[†] Jun Huang,[‡] and Xin Tu*[,†]

[†]Department of Electrical Engineering and Electronics, University of Liverpool, Liverpool L69 3GJ, United Kingdom

[‡]School of Chemical and Biomolecular Engineering, Sydney Nano Institute, The University of Sydney, Sydney, NSW 2037, Australia

Supporting Information

ABSTRACT: A better fundamental understanding of the plasma-catalyst interaction and the reaction mechanism is vital for optimizing the design of catalysts for ammonia synthesis by plasma-catalysis. In this work, we report on a hybrid plasma-enhanced catalytic process for the synthesis of ammonia directly from N_2 and H_2 over transition metal catalysts (M/Al_2O_3, M = Fe, Ni, Cu) at near room temperature (~35 °C) and atmospheric pressure. Reactions were conducted in a specially designed coaxial dielectric barrier discharge (DBD) plasma reactor using water as a ground electrode, which could cool and maintain the reaction at near-room temperature. The transparency of the water electrode enabled *operando* optical diagnostics (intensified charge-coupled device (ICCD) imaging and optical emission spectroscopy) of the full plasma discharge area to be conducted without altering the operation of the reactor, as is often needed when using coaxial reactors with opaque ground electrodes. Compared to plasma synthesis of NH_3 without a catalyst, plasma-catalysis significantly enhanced the NH_3 synthesis rate and energy efficiency. The effect of different transition metal catalysts on the physical properties of the discharge is negligible, which suggests that the catalytic effects provided by the chemistry of the catalyst surface are dominant over the physical effects of the catalysts in the plasma-catalytic synthesis of ammonia. The highest NH_3 synthesis rate of 471 μmol g^{-1} h^{-1} was achieved using Ni/Al_2O_3 as a catalyst with plasma, which is 100% higher than that obtained using plasma only. The presence of a transition metal (e.g., Ni) on the surface of Al_2O_3 provided a more uniform plasma discharge than Al_2O_3 or plasma only, and enhanced the mean electron energy. The mechanism of plasma-catalytic ammonia synthesis has been investigated through *operando* plasma diagnostics combined with comprehensive characterization of the catalysts using N_2 physisorption measurements, X-ray photoelectron spectroscopy (XPS), X-ray diffraction (XRD), high-resolution transmission electron microscopy (HRTEM), NH_3-temperature-programmed desorption (TPD), and N_2-TPD. Four forms of adsorbed NH_x (x = 0, 1, 2, and 3) species were detected on the surfaces of the spent catalysts using XPS. It was found that metal sites and weak acid sites could enhance the production of NH_3 via formation of NH_2 intermediates on the surface.

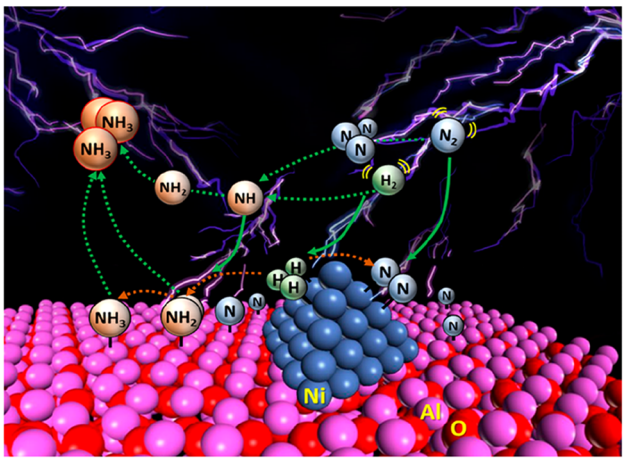

KEYWORDS: *nonthermal plasmas, plasma-catalysis, nitrogen fixation, ammonia synthesis, reaction mechanism*

1. INTRODUCTION

Ammonia is one of the most important chemicals used in modern society. It is a vital precursor in the synthesis of many useful products, including fertilizers, plastics, resins, explosives, and synthetic fabrics. It also has the potential to be used for energy storage[1−3] and as a hydrogen fuel.[4−6] It is produced on an industrial scale from N_2 and H_2 using the Haber-Bosch process, which is typically carried out at 450−600 °C and 150−300 bar in the presence of a highly active catalyst. This process emits over 300 million metric tons of CO_2 each year and is highly energy-intensive, consuming 1−2% of the world's primary energy supply: the largest in the chemical industry.[7,8] Moreover, as the demand for fertilizers for food crops increases with the ever-growing population, global production of ammonia is expected to increase 1−2% per year.[9,10] The continued use of the Haber-Bosch process to meet demands will lead to corresponding increases in energy consumption and CO_2 emissions, which will not only be environmentally and economically unfavorable, but will also make it difficult to meet European targets for reducing emissions.[11] Efforts have,

Received: June 17, 2019
Revised: October 16, 2019
Published: October 18, 2019

DOI: 10.1021/acscatal.9b02538
ACS Catal. 2019, 9, 10780−10793

therefore, been devoted to discovering greener, more efficient, and more economically sustainable alternatives to the Haber-Bosch process for small-scale ammonia production.[8,12,13]

Much of the energy expenditure of the Haber-Bosch process is due to the high temperatures and pressures required to synthesize ammonia from N_2 and H_2. High temperatures are needed to provide sufficient energy to dissociate the N_2 bond and drive the reaction. However, ammonia synthesis is an exothermic reaction and thermodynamically favorable at lower temperatures (eq 1), so high pressures are also needed to shift the equilibrium in favor of the ammonia production reaction because of Le Chatelier's principle. The key to reducing the energy consumption of ammonia synthesis processes is, therefore, in activating the N_2 bond at lower temperatures to avoid the requirement of high pressures.

$$3H_2 + N_2 \rightleftharpoons 2NH_3, \quad \Delta H_{298k} = -46.35 \text{ kJ mol}^{-1} \qquad (1)$$

Biochemical processes, electrochemical processes, and plasma processes with mild operating conditions are considered promising alternatives to thermal catalytic production of ammonia.[8,12,13] Of these, nonthermal plasma (NTP) is particularly attractive. NTPs generate highly energetic electrons and reactive species (e.g., radicals, excited atoms, molecules, and ions) that can significantly enhance reaction kinetics and enable thermodynamically unfavorable reactions to proceed under ambient conditions (e.g., dissociation of N_2).[14] Both the electrons and reactive species play a vital role in the initiation and propagation of a variety of physical and chemical reactions in low-temperature plasma processes.[15−17] A variety of NTPs have been investigated for ammonia synthesis, including dielectric barrier discharge (DBD),[18−21] pulsed streamer discharge, micro discharge,[22] radio frequency discharge,[23] and glow discharge[24] plasmas. Using NTP chemical processes for ammonia synthesis instead of the Haber-Bosch process could provide useful benefits: NTP reactions can be conducted under atmospheric conditions on a small-scale; they can be started and stopped very quickly by activating and deactivating the plasma; they have the flexibility to be combined with renewable energy sources, such as wind or solar power, to reduce the energy costs.[25] Hence, increasing efforts have been devoted to the use of NTP's for the synthesis of ammonia.[24,26−28]

Combining NTP's with heterogeneous catalysis (plasma-catalysis) demonstrably improves the performance of many plasma-activated reactions, including ammonia synthesis, CH_4 activation, CO_2 hydrogenation, and the water−gas shift reaction.[24,29−32] The enhancement in the reaction performance results from the synergy generated by the interaction between the plasma and the catalyst. The underlying mechanisms of the plasma-catalyst interactions are complex and not fully understood, though previous investigations have explored how the plasma is affected by changing the properties of the catalyst, and vice versa.[29,33−36] For instance, there is strong evidence to suggest that altering the physical properties of the catalyst material (e.g., dielectric constant, surface area, particle size, and void fraction) can modify the electric field, which subsequently alters the density and mode of the plasma discharge.[26] It has also been observed that the application of a plasma to a catalyst can change the chemical or electronic properties of the catalyst (e.g., in the metal oxidation state or work function), reduce catalyst poisoning, modify surface reaction pathways, or change the catalyst morphology by increasing the surface area or improving catalyst dispersion, all of which can enhance the catalyst performance.[33]

In recent years, increasing efforts have focused on the use of plasma-catalysis for ammonia synthesis at low temperatures. However, compared to thermal catalytic ammonia synthesis, only a few catalysts have been tested and evaluated in plasma-catalytic processes for ammonia synthesis. Sugiyama et al. demonstrated that coupling MgO and CaO basic metal oxides with a glow-discharge plasma provided catalytic activity in the production of ammonia, even though these catalysts are catalytically inactive in thermal ammonia synthesis.[24] Patil et al. investigated the effect of a range of supports—including γ-Al_2O_3, α-Al_2O_3, MgO, CaO, TiO_2, and quartz wool—on the synthesis of ammonia in a DBD reactor.[26] Mizushima et al. evaluated the effect of Al_2O_3 membrane-supported transition metal catalysts (Ru, Ni, Pt, and Fe) on the synthesis of ammonia using DBD plasma.[27] Mehta et al. investigated the plasma-catalytic synthesis of ammonia over a range of Al_2O_3 supported metal catalysts (Fe, Co, Ru, Rh, Pd, and Ni) in a DBD plasma reactor by evaluating experimental measurements with density functional theory (DFT) microkinetic modeling.[13] They have proposed that transition metals that bind nitrogen too weakly to be catalytically active in thermal reactions enhance the reaction rate more effectively in the plasma-catalytic reaction. The best turnover frequencies (TOFs) were found to occur on the step sites of weaker binding metals, such as Co and Ni catalysts, and on the terrace sites of stronger binding metals, like Ru.[13] Akay and Zhang tested microporous silica-supported nickel catalysts packed with $BaTiO_3$ spheres in the plasma-catalytic synthesis of ammonia in a DBD reactor at 130−150 °C.[28]

However, the knowledge of designing cost-effective, highly active, and stable catalysts that are effective in low-temperature plasma-catalytic synthesis of ammonia is still limited. A better fundamental understanding of the plasma-catalyst interactions and the reaction mechanism is required to optimize catalyst design for ammonia synthesis by plasma-catalysis. To this end, most of the previous works focused on the hybrid plasma process by tuning plasma processing parameters or using different catalysts; far less has been done to gain new insights into the role of these catalysts in the plasma-catalytic process. In this work, we have developed a plasma-enhanced catalytic process for the synthesis of ammonia directly from N_2 and H_2 at near-room temperature (~35 °C) and ambient pressure in a specially designed temperature-controlled DBD reactor that used water as a ground electrode. The water electrode provided two important functions: (i) the inherent transparency enabled optical diagnostics (intensified charge-coupled device (ICCD) imaging and optical emission spectroscopy) of the plasma and catalyst surface to be performed without disrupting the performance, uniformity, and operation of the plasma, as can happen with reactors with nontransparent ground electrodes (e.g., metal electrodes); (ii) water cooling can effectively remove heat generated by the discharge and maintain the reaction at near-room temperature (~35 °C) under different process conditions. To the best of our knowledge, such a plasma-catalytic reactor has not been used for ammonia synthesis at near-room temperature before. We aim to enhance the fundamental understanding of the role of a catalyst surface in plasma-catalytic ammonia synthesis at ambient conditions by combining *operando* electrical and optical diagnostics of the plasma reaction with comprehensive pre- and postreaction characterization of the catalyst surface.

DOI: 10.1021/acscatal.9b02538
ACS Catal. 2019, 9, 10780−10793

The reactions were conducted using three affordable and efficient Al_2O_3 supported metal (Ni, Cu, and Fe) catalysts. The performance of the water DBD reactor in the presence and absence of the catalysts was compared with the state of the art. A range of catalyst characterization techniques was used to understand how species generated in the plasma interacted with the catalyst surface to enhance ammonia production. A strong relationship between the acid sites on the catalyst surface and the rate of ammonia synthesis was identified, with higher rates of ammonia production occurring on the surface of catalysts that had a large number of weak acid sites. A plausible reaction mechanism for the plasma-catalytic ammonia synthesis is proposed based on the electrical and optical plasma diagnostics and characterization of the fresh and spent catalysts.

2. EXPERIMENTAL SECTION

2.1. Catalyst Preparation and Characterization. Five wt % M/Al_2O_3 (M = Fe, Ni, and Cu) catalysts were prepared by incipient wetness impregnation using nitrate salts (Alfa Aesar, 99.5%) as the metal precursor. Al_2O_3 catalyst support (3 g) was added to the solution of nitrate salts. The slurry was continuously stirred at 60 °C for 2 h, after which it was aged overnight at room temperature. The samples were then dried at 110 °C for 5 h and calcined at 500 °C for 5 h. The catalysts were then sieved to 40−60 mesh and reduced by Ar/H_2 mixed gas (100 mL min^{-1}; Ar/H_2 = 7:3) at 500 °C for 5 h before the plasma reaction. These catalysts, after reduction, will henceforth be referred to as "fresh catalysts".

N_2 physisorption measurements were carried out using a Quantachrome Autosorb-1 instrument at 77 K to determine the specific surface area, pore size distribution, average pore diameter, and average particle diameter for each of the catalysts. All catalysts, including the fresh catalysts and the spent catalysts, were pretreated at 300 °C under vacuum to remove any impurities from the surface.

X-ray diffraction (XRD) patterns of the fresh and spent catalysts were recorded by a Rigaku D/max-2200 diffractometer using a Cu Kα radiation source in the 2θ range from 20° to 80°.

High-resolution transmission electron microscopy (HRTEM) analysis of the fresh catalysts was carried out using a Tecnai G2 F20 microscope operating at an acceleration voltage of 300 kV. The catalyst samples were pretreated with ultrasonication in ethanol, then a drop of the resultant suspension was evaporated onto a carbon-coated copper grid. The particle size distribution of each catalyst was determined through the analysis of more than 300 particles from the TEM images.

X-ray photoelectron spectroscopy (XPS) analysis was performed on a Thermo ESCALAB 250Xi instrument using an Al Kα X-ray source calibrated with C_{1s} (284.8 eV). A low-resolution survey and high-resolution region scans were measured at the binding energy of interest for each of the spent catalysts.

The acidity of the catalysts was evaluated by temperature-programmed desorption (TPD) of ammonia and nitrogen (NH_3-TPD and N_2-TPD, respectively) using a Micrometrics AutoChem 2910 instrument equipped with a mass analyzer. For NH_3-TPD, 400 mg fresh catalysts were pretreated at 450 °C for 1 h then cooled to 50 °C. They were then exposed to NH_3 (5% vol.)/He at a flow rate of 30 mL min^{-1} until ammonia adsorption had reached equilibrium. Any physisorbed ammonia was removed by He (50 mL min^{-1}) at 100 °C. For the desorption tests, the samples were heated from 100 to 700 °C at 10 °C min^{-1}, and the amount of ammonia desorbed was measured by gas chromatographic (GC) quantification. For N_2-TPD, 100 mg of fresh catalysts were treated at 500 °C for 2 h under a flow of hydrogen, purged with He at 773 K for 1 h, and then cooled slowly over 2 h to 150 °C under an N_2 atmosphere. The samples were then cooled to room temperature under He flow (40 mL min^{-1}) to remove any physisorbed nitrogen. N_2-TPD was performed by heating the samples at a rate of 10 K min^{-1} from 50 to 500 °C.[37]

2.2. Experimental Setup. A schematic of the experimental setup is shown in Scheme. 1. The experiments were conducted

Scheme 1. Schematic Diagram of the Experimental Setup

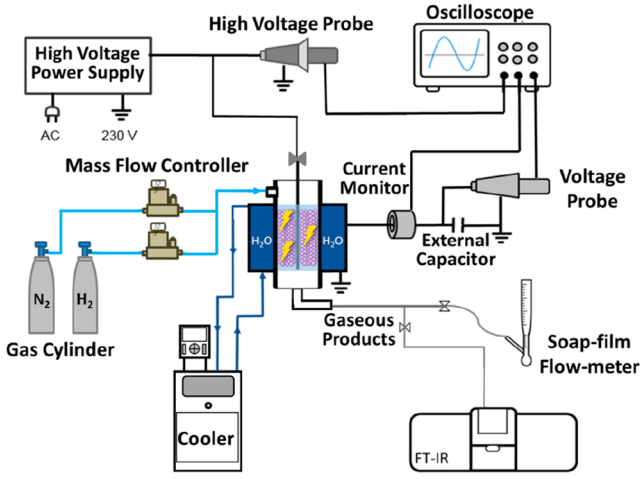

in a coaxial DBD reactor that used water as both a ground electrode and for controlling the temperature of the reactor. The water was circulated between two concentric quartz tubes, with the inner tube also functioning as a dielectric material for the reactor. The reaction temperature was maintained at 35 (±2) °C for the duration of the reaction using a cooling bath. In this special reactor design—compared to liquid—plasma or plasma-in-liquid reactors, where the plasma interacts with the liquid directly—the circulating water did not come into contact with the reactant or carrier gases during the reaction. The length of the discharge region was 50 mm, and the discharge gap was 2 mm. The DBD reactor was connected to an AC sinusoidal high voltage power supply with a peak-to-peak voltage of 24 kV and a frequency of 9.2 kHz. N_2 and H_2 were used as reactant gases at a constant total flow rate of 56 mL min^{-1} and an N_2/H_2 molar ratio of 1:2. The discharge area was fully packed with the catalyst (2 g). The plasma-catalyzed ammonia synthesis experiments were run for 6 h and the gas products were sampled every hour to monitor the performance of the different catalysts. Catalyst reuse experiments were conducted using Ni/Al_2O_3 as a catalyst, 2 h running time, and 30 min purging time between each test. The specific energy input (SEI) for each cycle was maintained at 26.8 kJ L^{-1}.

The applied voltage of the DBD was measured by a high-voltage probe (TESTEC, HVP-15HF), while the current was recorded by a current monitor (Bergoz, CT-E0.5). The voltage on the external capacitor (0.47 μF) was measured to determine the amount of charge accumulated in the DBD. All the

DOI: 10.1021/acscatal.9b02538
ACS Catal. 2019, 9, 10780−10793

electrical signals were sampled by a four-channel digital oscilloscope (Tektronix, MDO 3024). The discharge power was calculated using the Q-U Lissajous method and controlled by a real-time power monitoring system.[17] The gas temperature and the temperature of the catalyst bed (top, middle and bottom) in the discharge zone were measured using a fiber optic thermometer (Omega FOB102). The measured plasma gas temperature was almost the same as the temperature of the catalyst bed due to the effective cooling of the water electrode. In addition, the temperatures at different locations in the plasma-catalytic zone were almost the same (±2 °C). These findings show that the temperature-controlled DBD reactor using a water electrode can maintain the reaction temperature uniformly in the plasma-catalytic zone. Note that the reaction temperature can be maintained at ∼35 °C when changing the experimental conditions (e.g., SEI), which could be difficult when using a conventional DBD reactor.

The reaction products were analyzed using a Fourier transform infrared (FTIR) spectrometer (FTIR-4200, Jasco) with a resolution of 2 cm^{-1}. Each measurement was repeated three times, and the measurement error was less than 4%. The optical emission spectroscopy (OES) diagnostics of the N_2−H_2 DBD was performed using an optical fiber connected to a Princeton Instruments ICCD spectrometer (Model 320 PI) with a focal length of 320 nm (Figure S1). Gratings of 600 and 2400 g mm^{-1} were used to measure a wavelength range of 200−900 nm. Time-averaged optical imaging was performed by an ICCD camera (ANDOR iStar 334T) attached to a macro lens (Sigma Macro 105 mm F2.8 EX DG) with an exposure time of 50 ms to observe the plasma discharge behavior (Figure S1).

2.3. Calculation of Parameters. The specific energy input and ammonia synthesis rate (μmol h^{-1} g^{-1}) were calculated using eqs 2 and 3

$$\text{SEI (kJ L}^{-1}) = \frac{P_{\text{total}}}{Q_{\text{gas}}} \tag{2}$$

$$\text{NH}_3\text{ synthesis rate}(\mu\text{mol g}^{-1}\text{ h}^{-1}) = \frac{C_{\text{NH}_3} \times Q_{\text{gas}}}{m_c} \tag{3}$$

where P_{total} is the discharge power, Q_{gas} is the total gas flow, C_{NH3} is the concentration of ammonia generated in the plasma process, and m_c is the mass of fully packed catalysts (2 g).

The energy efficiency (g kWh^{-1}) was determined by eq 4

$$E_{\text{NH}_3}(\text{g kWh}^{-1}) = \frac{C_{\text{NH}_3} \times Q_{\text{gas-after}}}{P_{\text{total}}} \tag{4}$$

where $Q_{\text{gas-after}}$ is the volumetric gas flow rate after the reaction.

3. RESULTS

3.1. Fresh Catalyst Characterization. XRD patterns of the fresh catalysts are shown in Figure S2. Three major diffraction peaks centered at 2θ = 37.6°, 45.9°, and 67.0° were identified in the diffraction pattern of pure Al_2O_3, corresponding to the cubic structure of crystalline γ-Al_2O_3 (JCPDS 00-010-0425). These peaks were also found in the diffraction patterns of the M/Al_2O_3 catalysts. Peaks of metallic Fe (JCPDS 06-0696), Ni (JCPDS 45-1027), and Cu (JCPDS 04-0836) were present in the diffraction patterns of the corresponding fresh M/Al_2O_3 catalysts, indicating that the loaded metal species existed on the catalyst surface mainly in the metal state after thermal reduction.

Table 1 lists the physical properties of the fresh catalysts measured by N_2 physisorption. The Brunaur-Emmett-Teller

Table 1. Physical Characteristics of the Fresh Catalysts

samples	M loading (wt %)	surface area (m^2 g^{-1})	total pore volume (cm^3 g^{-1})	average particle diameter (nm)[a]
Al_2O_3		221	0.43	-
Ni/Al_2O_3	5	191	0.37	8.6
Fe/Al_2O_3	5	188	0.36	9.0
Cu/Al_2O_3	5	182	0.37	7.8

[a]Average particle diameter determined by HRTEM.[38]

(BET) specific surface area of fresh Al_2O_3 was 221 m^2 g^{-1}, while the specific surface areas of the fresh Al_2O_3-supported metal catalysts were smaller, between 182 and 191 m^2 g^{-1}. Fresh Al_2O_3 also had the most substantial total pore volume of 0.43 cm^3 g^{-1}, compared to 0.36−0.37 cm^3 g^{-1} for the M/Al_2O_3 catalysts. Figure 1 shows the surface morphology and particle size distribution of the fresh catalysts using HRTEM. Most of the metal particles on the catalyst surfaces were in the range of 2−16 nm, while the Fe/Al_2O_3 catalyst had several larger particles of around 40 nm. For the Ni/Al_2O_3 and Cu/Al_2O_3 catalysts, the metal particles were much more homogeneously dispersed over the surface of the support compared to Fe/Al_2O_3.[38]

The surface acidity of the fresh catalysts was determined by NH_3-TPD. Figure 2 shows the NH_3 chemical desorption peaks of weak (120−300 °C), medium (320−530 °C), and strong acid sites (550−730 °C).[39] For each catalyst, the amount of ammonia adsorbed on these sites is given in Table 2. It is clear that loading the Al_2O_3 support with metals reduced the total number of acid sites (A_{total}) by >50%, decreasing in the order: Al_2O_3 (0.97 mmol g^{-1}) > Ni/Al_2O_3 (0.46 mmol g^{-1}) > Cu/Al_2O_3 (0.45 mmol g^{-1}) > Fe/Al_2O_3 (0.33 mmol g^{-1}). There was also a notable reduction in the concentration of medium and strong acid sites (A_{medium}), and an increase in the concentration of weak acid sites with metal loading. Moreover, the temperature of desorption for all three acid sites decreased with metal loading−especially Cu and Ni. This indicated that the presence of metals not only reduced the number of acid sites, but also reduced the strength of the sites and, therefore, the overall surface acidity of the support.

The interactions between N_2 and the fresh M/Al_2O_3 catalyst surfaces were measured by N_2-TPD (Figure S3). The temperatures of the onset of desorption (T_{onset}) increased in the order: Ni/Al_2O_3 (285 °C) < Cu/Al_2O_3 (290 °C) < Fe/Al_2O_3 (302 °C). The lowest T_{onset} was achieved with Ni/Al_2O_3 at 285 °C, indicating that some N_2 was more weakly bound to the surface Ni/Al_2O_3 than the other catalysts.

3.2. Plasma Synthesis of Ammonia over Transition Metal Catalysts. A comparison of the different catalyst performances−with regards to NH_3 synthesis rates and yields, at an SEI of 26.8 kJ L^{-1} is shown in Figure 3a. The use of Al_2O_3 support with DBD showed a notable improvement in the rate of ammonia synthesis compared to the reaction without catalyst (plasma only). The presence of a transition metal supported on Al_2O_3 further enhanced the synthesis rate, with the catalyst activity decreasing in the order: Ni/Al_2O_3 > Cu/Al_2O_3 > Fe/Al_2O_3 > Al_2O_3 > plasma only. Ni/Al_2O_3 gave

DOI: 10.1021/acscatal.9b02538
ACS Catal. 2019, 9, 10780−10793

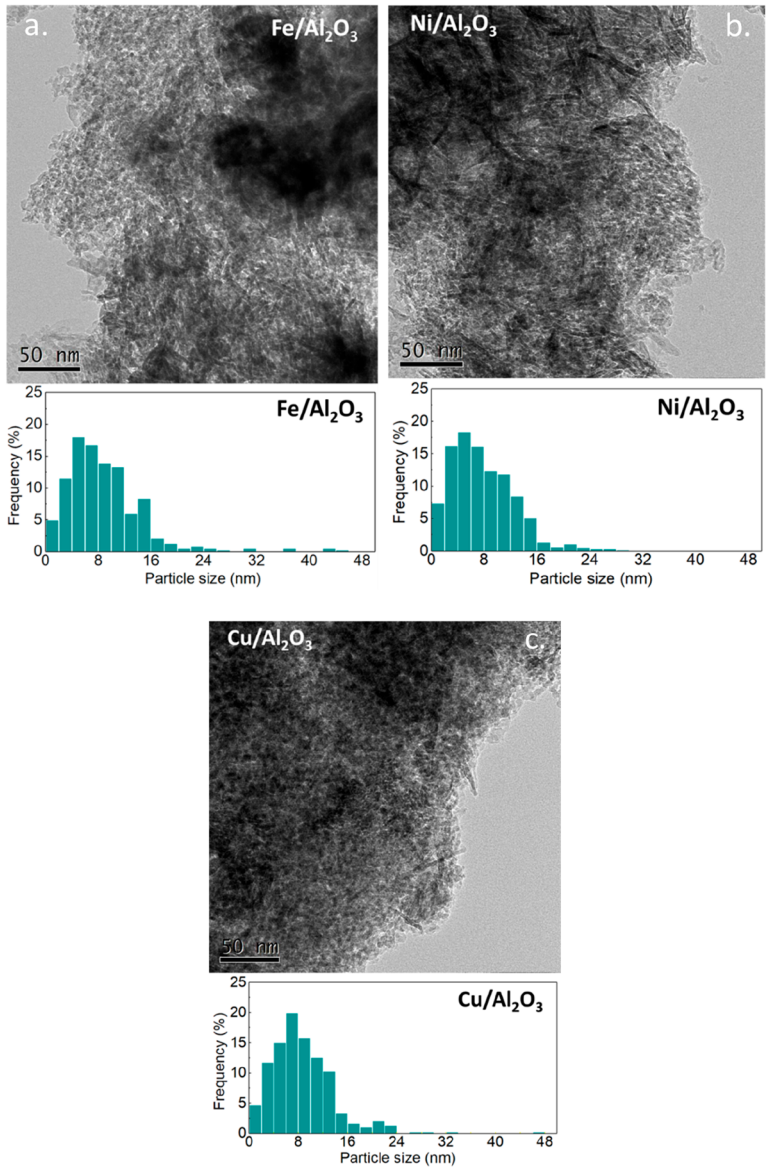

Figure 1. HRTEM images with the distribution of the particle size (0−50 nm) of the fresh catalysts after reduction (a) Fe/Al_2O_3, (b) Ni/Al_2O_3, and (c) Cu/Al_2O_3.

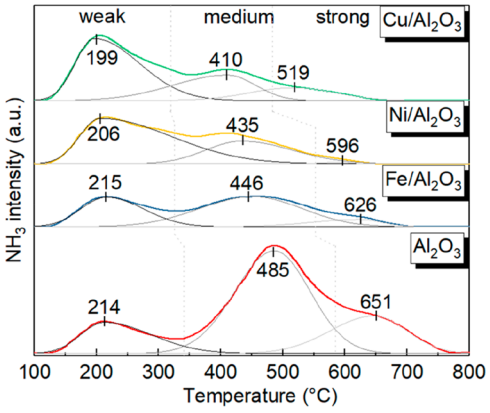

Figure 2. NH_3-TPD profiles of the fresh catalysts.

the best synthesis rate of 390 μmol g^{-1} h^{-1} and a yield of 0.77%, whereas Fe/Al_2O_3 only slightly enhanced the NH_3 synthesis rate compared to Al_2O_3. The observed trend in

Table 2. Surface Acidity of the Fresh Catalysts

	NH_3-TPD		
catalyst	A_{weak} [a] (mmol g^{-1})	A_{medium} [b] (mmol g^{-1})	A_{total} [c] (mmol g^{-1})
Al_2O_3	0.30	0.78	0.97
Fe/Al_2O_3	0.17	0.16	0.33
Ni/Al_2O_3	0.38	0.08	0.46
Cu/Al_2O_3	0.36	0.09	0.45

[a] A_{weak} is the concentration of weak acid sites. [b] A_{medium} is the concentration of medium + strong acid sites. [c] A_{total} is the total concentration of acid sites on the catalyst surface

activity may have been due to stronger adsorption of N_2 species on Fe active sites than on the other transition metals or active surface sites. This has been reported in previous works to slow down the rate of ammonia synthesis by increasing the activation energy barrier for hydrogenation.[13] All the catalysts showed excellent stability in performance over 6 h without any deactivation (Figure 3c). Also, as shown in Figure 3d, both the

DOI: 10.1021/acscatal.9b02538
ACS Catal. 2019, 9, 10780−10793

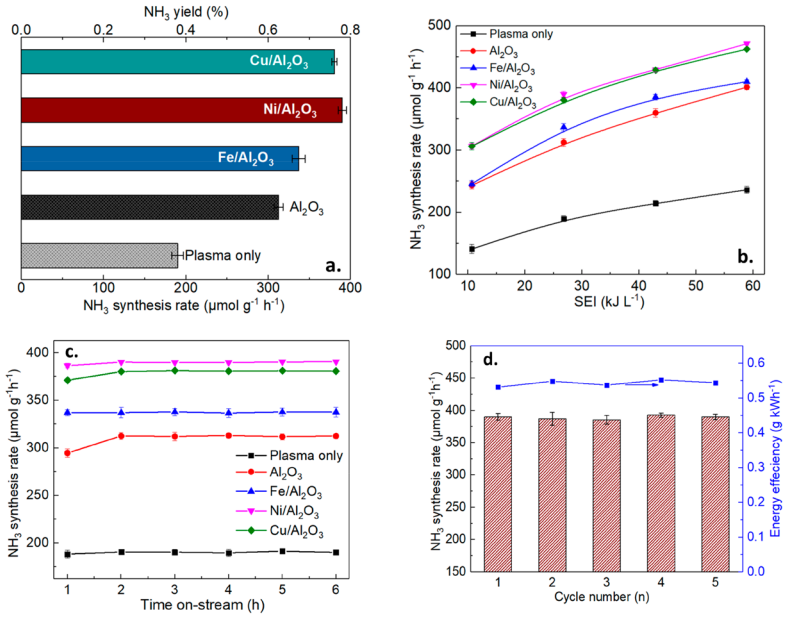

Figure 3. Evaluation of catalyst activities for ammonia synthesis. (a) NH_3 synthesis rates and NH_3 yield at an SEI of 26.8 kJ L^{-1}. (b) SEI dependence of the NH_3 synthesis rate using different catalysts. (c) Stability for different catalysts. (d) Catalyst reuse experiments over Ni/Al_2O_3 in NH_3 synthesis with the rates and energy efficiencies at an SEI of 26.8 kJ L^{-1}.

NH_3 synthesis rate and the energy efficiency of Ni/Al_2O_3 remained constant over 5 reuse cycles. This provided a good indicator of the long-term stability of the catalysts in the reaction.

The influence of the catalysts on the NH_3 synthesis rate at different SEI is shown in Figure 3b. SEI was altered by varying the discharge power at a constant total flow rate; Note that the use of a water electrode was able to maintain the reaction temperature at ~35 °C when changing the SEI. The rate increased considerably as the SEI increased, regardless of which catalyst was used; for instance, the NH_3 synthesis rate increased from 306 to 471 μmol g^{-1} h^{-1} when the SEI increased from 10.7 to 58.9 kJ L^{-1} in the presence of Ni/Al_2O_3 catalyst. This is most likely because increasing the discharge power generated more active species in the plasma that can react to form ammonia. The effect of SEI on the energy efficiency of the plasma process using different catalysts is shown in Figure S8. The energy efficiency for ammonia synthesis greatly dropped when increasing the SEI, again regardless of which catalyst was used. Increasing the discharge power of a plasma produces more energetic electrons that can interact with atoms and molecules to generate active species for ammonia synthesis. As the SEI increases, the ratio of energetic electrons to atoms/molecules in the discharge zone increases, resulting in more electron-atom/electron-molecule interactions and the production of more active species; however, a greater proportion of electrons will not participate in effective collisions and their energy is wasted, thus reducing the energy efficiency of the process. Compared to the plasma only reaction, packing the DBD with a catalyst enhanced the energy efficiency for the synthesis of ammonia, especially for Ni/Al_2O_3 and Cu/Al_2O_3, which showed the joint-highest energy efficiencies at each SEI.

The results of the best catalytic performance obtained in this work, using Ni/Al_2O_3 as a catalyst, are compared with the catalytic performances of other Ni-based catalyst systems for plasma-enhanced ammonia synthesis from the literature in Table S4. Akay et al. achieved an energy efficiency of 0.57 g kWh^{-1} using a mixture of Ni/SiO_2 and $BaTiO_3$, which was almost double that obtained in this work; however, 173 g of catalyst was required in their reaction, whereas only 2 g of catalyst was used in our system.[28] Iwamoto et al. achieved the highest synthesis rate of 1920 μmol h^{-1}, but with a much lower energy efficiency of 0.02 g kWh^{-1}.[40] Our Ni/Al_2O_3 catalyst with a water-cooled electrode DBD system, therefore, provided a competitive ammonia synthesis rate and good energy efficiency using only a small amount of catalyst.

3.3. Evaluation of the Spent Catalysts after Reaction.

It is well-known that the physicochemical properties of catalysts can be changed after their use in plasma reactions.[41] To investigate the effect of plasma-catalytic ammonia synthesis on the catalysts used in this work, spent catalysts were collected after they were used for ammonia synthesis with plasma at an SEI of 26.8 kJ L^{-1} for 90 min. A comparison of the physicochemical properties of the fresh and spent (after reaction) catalysts, as determined by N_2-physisorption measurements, are shown in Table S1. The specific surface areas of the spent catalysts (158−200 m^2 g^{-1}) were smaller than those of the fresh catalysts (182−221 m^2 g^{-1}), the total pore volumes of the spent catalysts had decreased from 0.36−0.43 (fresh catalysts) to 0.32−0.39 cm^3 g^{-1}, and the average pore diameters of the spent catalysts increased by 0.5−2.4% after the plasma reaction. These observations could be attributed to the collapse of microchannels in the catalyst structure by the collision of energetic particles.[41] The nitrogen isotherms of the fresh and spent catalysts are compared in Figure 4. All samples exhibited type-IV isotherms with H1 hysteresis loops and steep increases in the relative pressure range of $0.5 < P/P_0 < 0.9$, indicating that all of the samples had mesoporous structures.[42,43] This suggests that the reactions in plasma did not have a significant impact on the main pore structures of the catalysts.

The surface acidity of fresh and spent samples of the best performing catalyst, Ni/Al_2O_3, were evaluated by NH_3-TPD.

DOI: 10.1021/acscatal.9b02538
ACS Catal. 2019, 9, 10780−10793

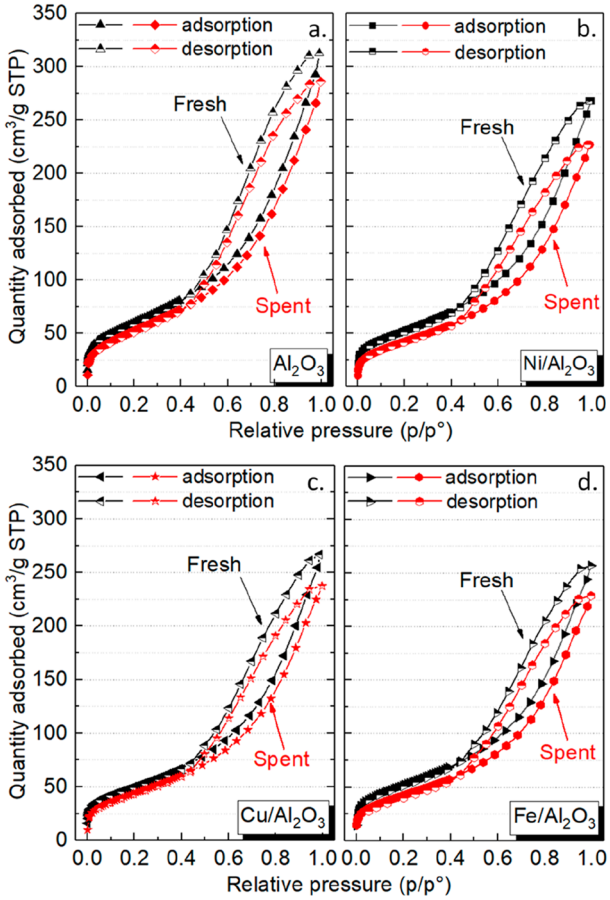

Figure 4. N_2 adsorption−desorption isotherms of (a) Al_2O_3, (b) Fe/Al_2O_3, (c) Ni/Al_2O_3, and (d) Cu/Al_2O_3.

The results are shown in Figure 5. The concentration of acid sites was lower on the surface of the spent catalyst than on the

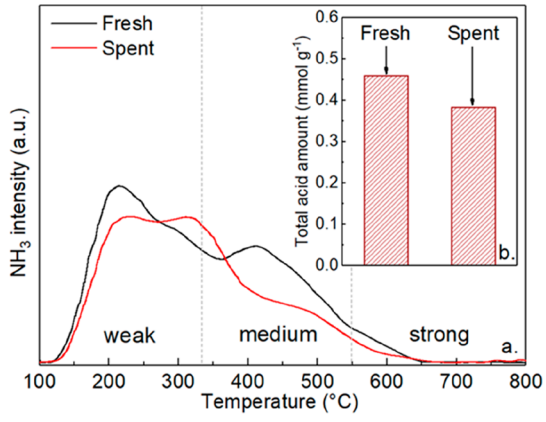

Figure 5. (a) NH_3-TPD profiles for fresh and spent Ni/Al_2O_3. (b) Comparison of total acid amounts for fresh and spent Ni/Al_2O_3.

fresh catalyst (Figure 5b), indicating that some sites had been lost during the reaction. This corresponds with the loss of surface area (see Table S1). A new peak is present in the results for the spent catalyst at a desorption temperature of 320 °C (Figure 5a), which suggested that a new type of acid site had been produced on the catalyst surface during the reaction that was more acidic than the weak sites and less acidic than the medium sites on the surface of the fresh catalyst. The alteration to the sites is likely the result of interactions and collisions with excited particles produced in the plasma.[41]

XPS measurements were conducted to detect the presence of NH_x (where x = 0, 1, 2, or 3) species on the surface of the spent catalysts. The results of the N 1s core level measurements for each catalyst are shown in Figure 6a, while the

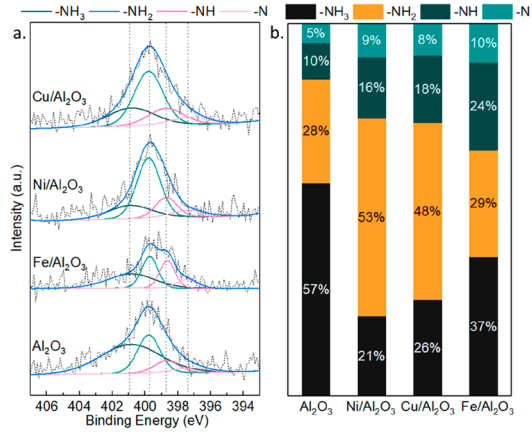

Figure 6. (a) N 1s core level measurements for Al_2O_3, Ni/Al_3O_3, Cu/Al_2O_3, and Fe/Al_2O_3 after reaction in N_2−H_2 plasma, and (b) proportion of individual peaks assigned to NH_x (where x = 0, 1, 2, or 3).

proportions of the individual peaks assigned to NH_x species are given in Figure 6b and Table S2. The assignments for the NH_x peaks were determined from the literature.[44−46] The concentrations of adsorbed NH_3 and NH_2 were inversely proportional to each other, with the concentration of NH_3 decreasing in the order: Al_2O_3> Fe/Al_2O_3> Cu/Al_2O_3> Ni/Al_2O_3 and the concentration of NH_2 increasing in the order: Ni/Al_2O_3> Cu/Al_2O_3 > Fe/Al_2O_3 > Al_2O_3. Higher proportions of NH and N were detected on the surface of Fe/Al_2O_3 than on the other catalysts, signifying that these species were more stable on the surface of Fe/Al_2O_3, making them slightly less reactive, and thus slower to form ammonia. Lower concentrations of N on the surfaces of Ni/Al_2O_3 and Cu/Al_2O_3 may indicate that less direct N_2 dissociation occurs on their surfaces than on the surface of Fe/Al_2O_3. Instead, weakly adsorbed vibrationally active N_2 species may be more important for ammonia synthesis on their surfaces. Despite there being only small concentrations of NH_x species detected on the surface of the spent catalyst, these relationships may provide an insight into the importance of these species in surface-mediated reactions in atmospheric pressure, non-thermal plasma-catalytic ammonia synthesis reactions, as discussed in section 4 of this paper.

3.4. Plasma Characterization for NH_3 Synthesis Using Al_2O_3 and Ni/Al_2O_3 Catalysts. The plasmas produced in N_2−H_2 gas using different reactor configurations (plasma only, Al_2O_3 and Ni/Al_2O_3) were characterized using ICCD and BOLSIG+ calculations.[47] Note that there were no obvious changes to the discharge properties when packing the discharge area with different M/Al_2O_3 catalysts; therefore, only the results for the catalyst that gave the best performance in plasma-catalytic synthesis of ammonia, Ni/Al_2O_3, will be discussed here.

Images of the discharge areas of unpacked, Al_2O_3-packed and Ni/Al_2O_3-packed reactor configurations, are shown with

DOI: 10.1021/acscatal.9b02538
ACS Catal. 2019, 9, 10780−10793

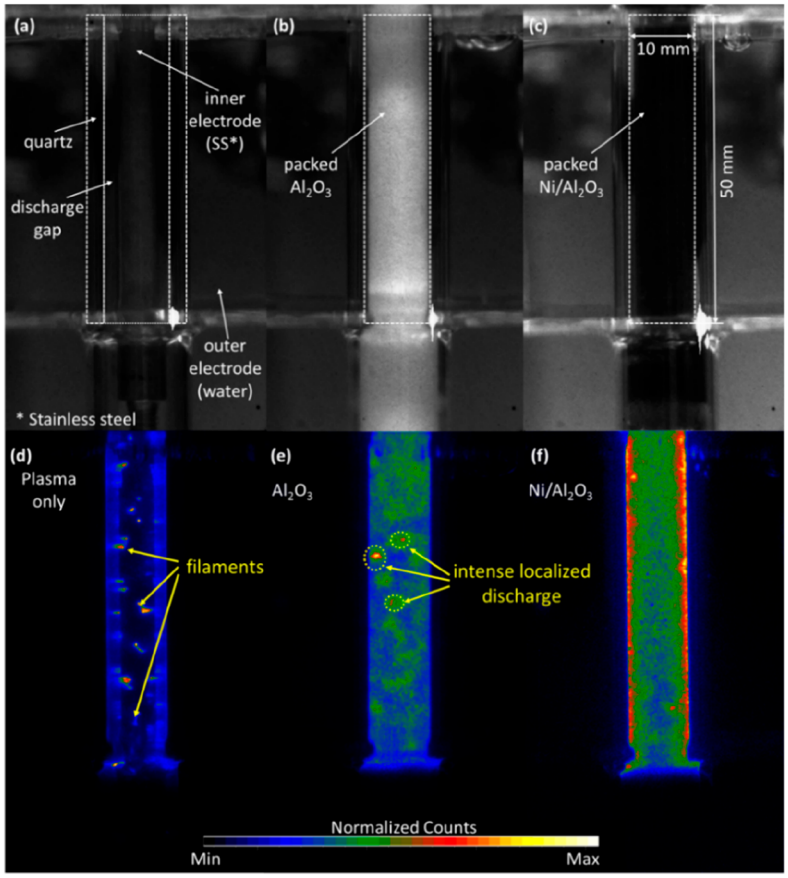

Figure 7. ICCD camera images of the unpacked reactor, packed with Al_2O_3 and Ni/Al_2O_3; (a–c) images without discharge; (d–f) photos with discharge (exposure time: 50 ms).

the plasma off in Figure 7a–c, respectively. The time-averaged ICCD images presented in Figure 7d–f show the emission in the discharge area. Figure 7d shows typical filaments were produced in the discharge area in the absence of packing material. Filling the entire discharge gap with Al_2O_3 or Ni/Al_2O_3 (Figure 7e and f, respectively) significantly reduced the gas void in the plasma-catalyst zone. This reduces the generation of filamentary discharges while enhancing the formation of surface discharges due to the presence of catalyst surfaces in the discharge area, which has been well demonstrated in both experimental and modeling studies of packed bed DBD reactors.[16,48,49] This phenomenon can also be confirmed from the difference of current discharge signals using unpacked and packed discharges. As shown in Figure S5c, compared to the discharge without a catalyst, the current pulses appear denser in the discharge packed with Al_2O_3 or Ni/Al_2O_3 due to the presence of more surface discharge with catalyst packing. The number of current pulses with an amplitude larger than 30% of the peak current in one period (Figure S5c) was determined, after extracting the sinusoidal displacement current, by using an asymmetric least-square method. The number of current pulses in the DBD packed with Al_2O_3 and Ni/Al_2O_3 are 2.3 and 2.9 times higher than that without packing catalysts, respectively. Compared to the discharge packed with Al_2O_3 only, the coupling of the DBD with Ni/Al_2O_3 promoted the expansion of the discharge and inhibited the formation of intense localized discharge in the plasma-catalyst zone. This is due to the presence of conductive Ni nanoparticles on the surface of the catalyst. A similar phenomenon was also observed in previous works.[50,51]

To further understand the characteristics of the discharges produced in the different reactor configurations, electrical diagnostics were carried out and a number of discharge parameters were calculated using electrical signals together with the U-Q Lissajous figures (Table 3 and Figure 8a–c).[52]

Table 3. Discharge Properties for Plasma Only, Packed with Al_2O_3 and Ni/Al_2O_3 (SEI of 26.8 kJ L^{-1})

	E (kV cm^{-1})	E/N (Td)	n_e[a] ($\times 10^{18}$, m^{-3})
plasma only	14.7 ± 0.3	61.6 ± 1.4	1.47 ± 0.04
Al_2O_3	18.5 ± 0.1	77.6 ± 0.5	1.10 ± 0.02
Ni/Al_2O_3	19.3 ± 0.1	81.0 ± 0.5	1.21 ± 0.02

[a]The calculation of n_e (mean electron density) is described in the Supporting Information.

The method for calculating the reduced electrical field (E/N) is given in section 5 of the Supporting Information. The presence of the packing materials in the discharge area enhanced the average electric field (E) from 14.7 kV cm^{-1} with plasma only to 18.5 kV cm^{-1} and 19.3 kV cm^{-1} with Al_2O_3 or Ni/Al_2O_3 packing, respectively, although the shape of Lissajous figures was almost the same (Figure 8a–c). The notable improvement in the average electric field produced by packing is likely the result of increased charge deposition. This is due to more effective polarization at the contact points of the packing particles with increasing dielectric constant of the materi-

DOI: 10.1021/acscatal.9b02538
ACS Catal. 2019, 9, 10780–10793

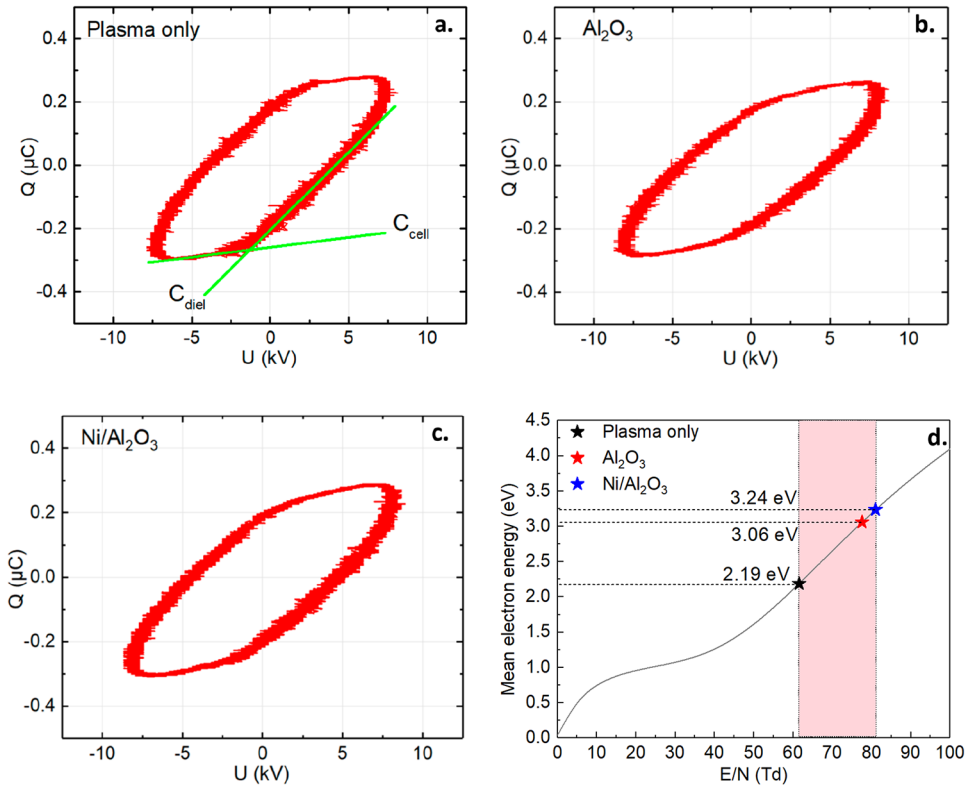

Figure 8. Lissajous figures of plasma only (a), packed with Al_2O_3 (b), and Ni/Al_2O_3 (c) (SEI of 26.8 kJ L^{-1}; C_{cell}, ζ_{diel}: illustrated in the Supporting Information). (d) Calculated mean electron energy for plasma only, packed with Al_2O_3 and Ni/Al_2O_3.

als.[16,52−55] The mean electron energy and the electron energy distribution function (EEDF) were calculated with the Boltzmann equation using BOLSIG+.[47] The order of the mean electron energies was Ni/Al_2O_3 (3.24 eV) > Al_2O_3 (3.06 eV) > plasma only (2.19 eV; Figure 8d), which corresponds with the enhancement of the electric field (see Figure 8). Furthermore, a plot of the electron energy distribution functions against the mean electron energies (Figure S7) shows that packing the discharge area with Ni/Al_2O_3 generated more electrons with higher energies, especially above 2.24 eV. However, the mean electron density (n_e, Table 3) of the discharge slightly decreased with the inclusion of packing materials.

The relationship between the rate coefficients and the reduced electric field (E/N) for the most common electron impact reactions in N_2−H_2 plasma were calculated using BOLSIG+, as shown in Figure 9. The rate coefficients for all of the reactions increased with increasing E/N. In the presence of catalysts, the reaction rates increased in the order: Ni/Al_2O_3 > Al_2O_3 > plasma only, in line with the increasing E/N and mean electron energy of the plasma (Figure 8d). These results suggest that increasing E/N and the mean electron energy increased the frequency of effective electron impact reactions to generate radicals and vibrationally excited species (see Figure 9) that can react to produce ammonia.

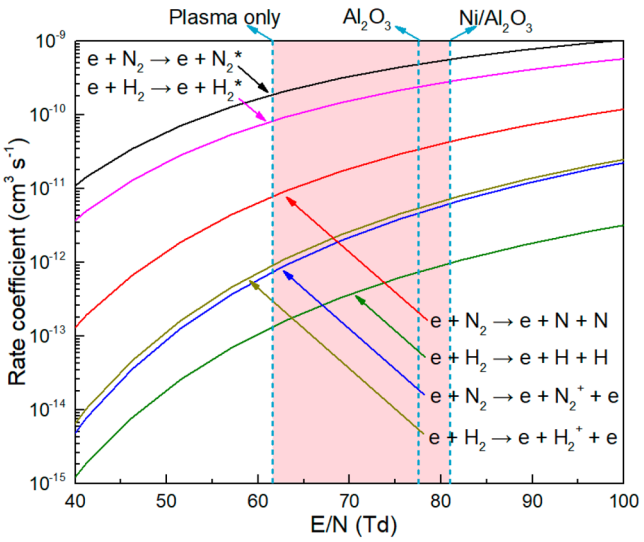

Figure 9. Rate coefficients of electronic excitation reactions calculated using BOLSIG+ (only gas phase).

4. DISCUSSION

4.1. Correlation of Acid Sites to the Ammonia Synthesis. The relationship between the concentrations of weak and medium + strong acid sites against $\log_{10}$ of the turnover frequency for each M/Al_2O_3 catalyst is shown in Figure 10. The TOF increased with increasing concentration of weak acid sites and decreased with increasing concentration of medium + strong acid sites. The highest TOF was achieved with Ni/Al_2O_3 (2.16×10^{-3} s^{-1}), which had the highest concentration of weak acid sites and the lowest concentration of medium + strong acid sites. The lowest TOF was obtained with Fe/Al_2O_3 (1.63×10^{-3} s^{-1}), which had the lowest concentration of weak acid sites and the highest concentration of medium + strong acid sites. These results indicate that there is a direct correlation between catalyst performance and the strength of the acid sites on the surface. To better understand

DOI: 10.1021/acscatal.9b02538
ACS Catal. 2019, 9, 10780−10793

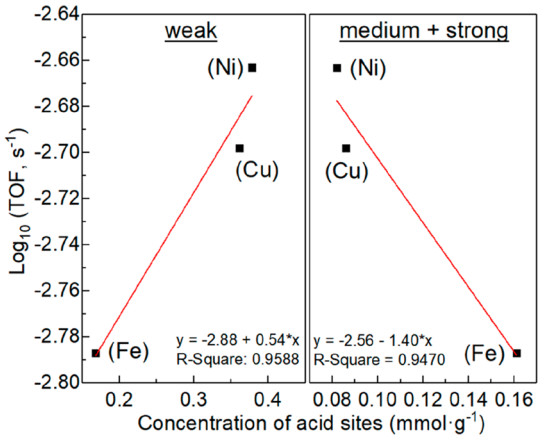

Figure 10. Correlation between $\log_{10}$ (TOF, s^{-1}) with weak and medium + strong acid sites.

these results, the reactions and adsorbed species on the catalysts were investigated.

The equations for many of the known reactions that can occur in the plasma-catalytic synthesis of ammonia from the literature are compiled in Table S5. Reactions that take place on the catalyst surface are believed to significantly enhance the reaction rate via interactions between the reactants and active metal and acid sites on the surface of the catalyst.[23] These active sites operate by providing multiple functions: they can adsorb active species (e.g., NH_x, H_a, N_2^+, etc.) from the plasma phase onto the surface to improve the localized concentration of reactants (eqs S1−S4), they can aid dissociation of adsorbed molecular species to more active intermediate species (equations S16−S19), and they can facilitate reactions with adsorbed species (eqs S5−S15) to promote NH_3 synthesis. It was proposed by Shah et al. that surface-adsorbed NH_2(s) is the most important intermediate in the production of ammonia.[23] NH_2 (s) is formed in situ by direct adsorption of NH_2 onto the surface from the gas-phase, reactions between NH radicals from the gas phase with surface adsorbed species, and reactions with surface adsorbed NH via both the Eley−Rideal (E-R) mechanism (Table S5, eq S6: NH + H (s) → NH_2 (s)) and the Langmuir−Hinshelwood (L-H) mechanism (eq S13: NH (s) + H (s) → NH_2 (s) + Surf), respectively. The most active catalyst used in this work, Ni/Al_2O_3, had the highest proportion of NH_2 groups detected on its surface after the reaction (Figure 6) and the highest concentration of weak acid sites (Table 2); therefore, the relationship between the proportion of NH_2 and the concentration of weak acid sites on the different catalyst surfaces was investigated (Figure 11a). The proportion of adsorbed NH_2 increased as the concentration of weak acid sites increased in the order: Ni/Al_2O_3 > Cu/Al_2O_3 > Fe/Al_2O_3 > Al_2O_3, which also follows the order of catalytic activity in ammonia production (Figure 3). These findings indicate that formation of the NH_2 intermediates was enhanced by the presence of weak acid sites on the surface of the catalyst. The weak surface interactions likely aided the migration of adsorbates across the catalyst surface to active sites (e.g., M sites) to react via L-H mechanisms. Moreover, the acid sites themselves probably functioned as active sites for ammonia synthesis, as is evident from the activity of the Al_2O_3 support with plasma in the absence of transition metals. The weaker surface interactions may have also enabled more facile desorption of NH_3 from the surface, which freed up surface

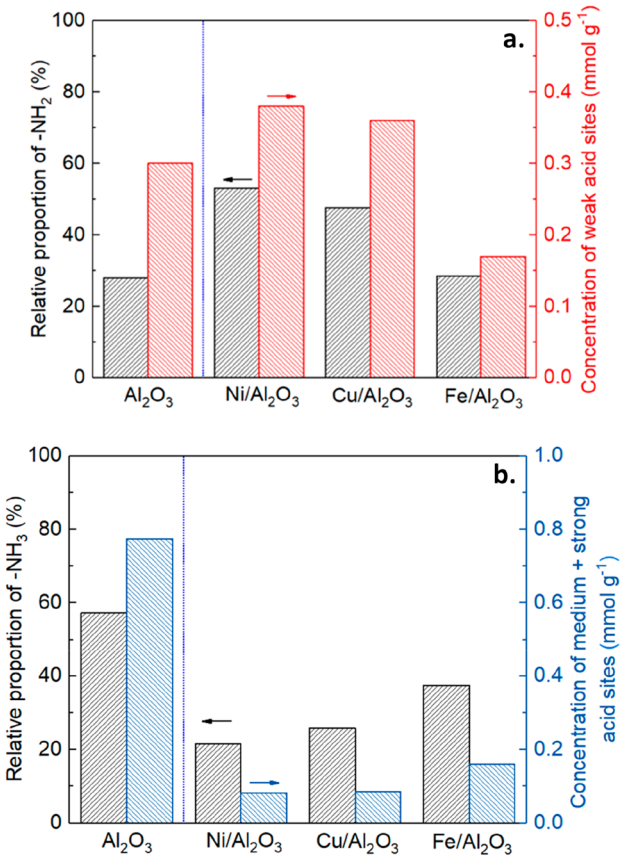

Figure 11. (a) Comparison of the relative proportion of NH_2 and concentration of weak acid sites on M/Al_2O_3 surfaces and (b) comparison of the relative proportion of NH_3 and concentration of strong + medium acid sites on M/Al_2O_3 surfaces.

sites and provided faster turnover with fresh reactants. Indeed, the strong acidity of oxide supports is known to be detrimental to the performance for ammonia synthesis as this binds ammonia more robustly to the surface.[56] This argument is supported by comparing the observed relationship between the proportion of adsorbed NH_3 vs. the concentration of medium + strong acid sites on the catalyst surface (Figure 11b) with the catalyst performances. The proportion of adsorbed NH_3 increased with increasing concentration of medium and strong acid sites (Table 2) in the order: Al_2O_3 > Fe/Al_2O_3 > Cu/Al_2O_3 > Ni/Al_2O_3, whereas the catalyst activity decreased in the order: Ni/Al_2O_3 > Cu/Al_2O_3 > Fe/Al_2O_3 > Al_2O_3. The stronger NH_3 binds to the surface, the more slowly NH_3 desorption from the surface occurs, which inhibits the availability of active sites and slows the rate of ammonia synthesis. Moreover, stronger binding of NH_3 to the surface of the catalyst increases its retention time in the plasma discharge area, which increases the probability of plasma-catalytic degradation of NH_3 occurring, thus reducing yield and the apparent (measured) rate of synthesis.

4.2. Enhancement Mechanism of Ni/Al_2O_3. Optical emission spectra of the N_2−H_2 DBD were measured to better understand the formation and role of gas-phase active species in the plasma-enhanced synthesis of ammonia using different reactor configurations (Figure S9). The existence of N_2 ($C^3\Pi_u \rightarrow B^3\Pi_g$) second positive system (SPS) and weak band of N_2 ($B^3\Pi_g \rightarrow A^3\Sigma_u$) first positive system (FPS)[23] in the spectra suggested the presence of electronically excited nitrogen (R1: e

DOI: 10.1021/acscatal.9b02538
ACS Catal. 2019, 9, 10780−10793

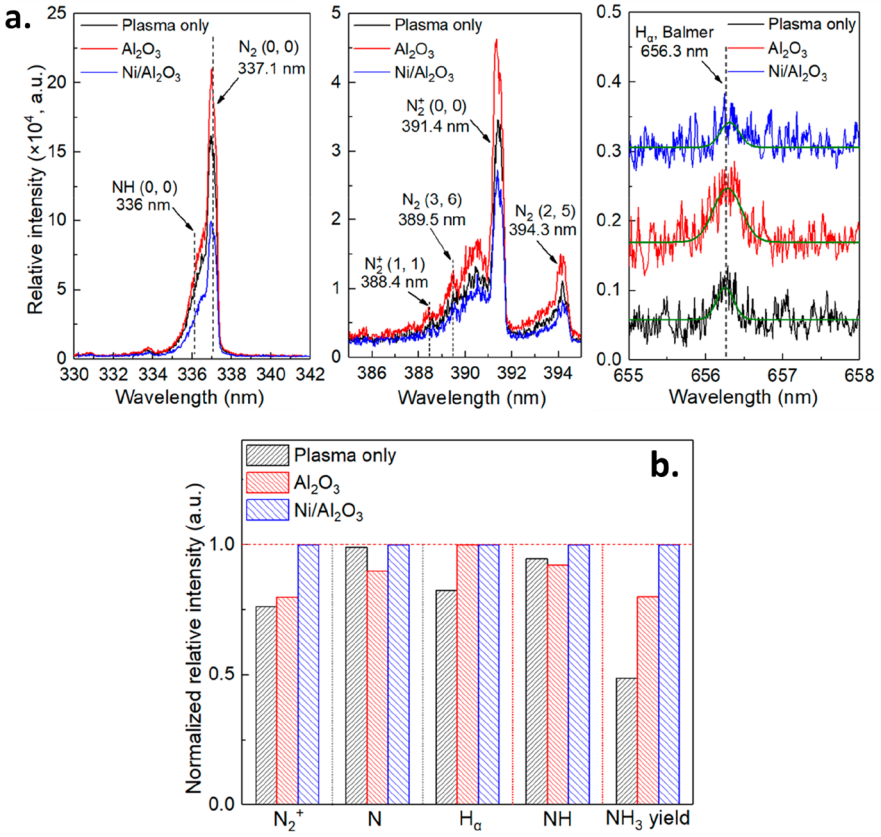

Figure 12. (a) Emission spectrum of NH, N_2, N_2^+, and H_α for plasma only, packed with Al_2O_3 and Ni/Al_2O_3 (exposure time: 600 ms); (b) normalized relative intensity of N_2^+, N, H_α, and NH (SEI of 26.8 kJ L^{-1}).

+ $N_2 \rightarrow e + N_2^*$, Table S5).[23,57] The presence of $N_2^+(B^2\Sigma_u^+ \rightarrow X^2\Pi_g^+)$ first negative system (FNS) indicates that the ionization of nitrogen (R2: $e + N_2 \rightarrow e + N_2^+ + e$) took place in the reaction. Identification of N ($3p^2P_0$-$3s^2P$) atomic lines (674.0 nm) and H_α Balmer atomic line (656.3 nm) suggests the dissociation of N_2 and H_2 (R3, R6).[58] The NH band head at 336 nm also could be identified as a shoulder peak beside N_2 (0, 0) (Figure 12a).[23]

The normalized relative intensities of N_2^+, N, H_α, and NH for plasma only, and Al_2O_3 and Ni/Al_2O_3 packed configurations are shown in Figure 12b (for the explanation on how the intensities were normalized, see Supporting Information section 9.2). The intensities for N_2^+, N, H_α, and NH were at relative maxima with the Ni/Al_2O_3 catalyst, indicating that this configuration could promote the generation of more excited species and radicals. The order of signal intensity for the largest peak, N_2^+, was Ni/Al_2O_3 > Al_2O_3 > plasma only, which corresponds with the order of the mean electron energy values (Figures 12b and 8d)[59] and increasing uniformity of the plasma discharge (Figure 7). Similarly, there is a remarkable increase in the intensity of the H_α atomic line with Al_2O_3 and Ni/Al_2O_3 packing, indicating that more H atoms were generated, possibly due to the dissociation of a greater portion of H_2 molecules with increasing the mean electron energy (Figures 12b and 8). Furthermore, when comparing the spectra of the different packed catalysts, there were notable variations in the intensity of the NH band head at 336 nm with changes in the N_2^+, N and H_α signal strengths. Both N_2^+ and NH signal intensities were higher in the Ni/Al_2O_3 spectrum than those in the plasma only and Al_2O_3 spectra, while the intensities of the N and H_α peak signals followed the orders Ni/Al_2O_3 > plasma only > Al_2O_3 and $Ni/Al_2O_3 \approx Al_2O_3$ > plasma only, respectively. These results suggest that more NH was produced with Ni/Al_2O_3 due to higher ratios of N_2^+, N and H formed in the plasma discharge. Indeed, it has been proposed in previous works that NH radicals are generated from these species in the plasma.[60−62] Moreover, Hong et al. found that NH radicals are a critical species in the initiation and acceleration of ammonia synthesis. They are important in the gas-phase generation of NH_3 in the plasma and are involved in three-body reactions (R19−R22) with N_2 and H_2 molecules.[61] The more NH radicals that are involved in these reactions, the faster the production of ammonia in the gas phase.

As discussed previously, $NH_2(s)$ has been identified in other works as an important species in the formation of ammonia, which itself is formed through the gas-phase and surface-adsorbed NH species through E-R and L-H reactions, respectively. The higher concentration of NH radicals produced in the plasma with Ni/Al_2O_3 may, therefore, contribute to the improved yield and synthesis rate of ammonia by increasing the concentration of $NH_2(s)$.

Wang et al. stated that the dissociative adsorption of NH_3 on the catalyst surface (S20−S22) would occur more easily with a stronger M-N bond.[63] An indication of the relative strength of the M-N (M: metal, including Fe, Ni, Cu) bond for the different catalysts used in this work was determined by T_{onset}, measured by N_2-TPD, which increased in the order: Ni-N < Cu-N < Fe-N. The observed order in ammonia yield with M/Al_2O_3 catalysts, Ni/Al_2O_3 > Cu/Al_2O_3 > Fe/Al_2O_3, is in line

DOI: 10.1021/acscatal.9b02538
ACS Catal. 2019, 9, 10780−10793

Scheme 2. Proposed Mechanism for the Enhancement of Ammonia Synthesis by Ni/Al_2O_3 Catalyst

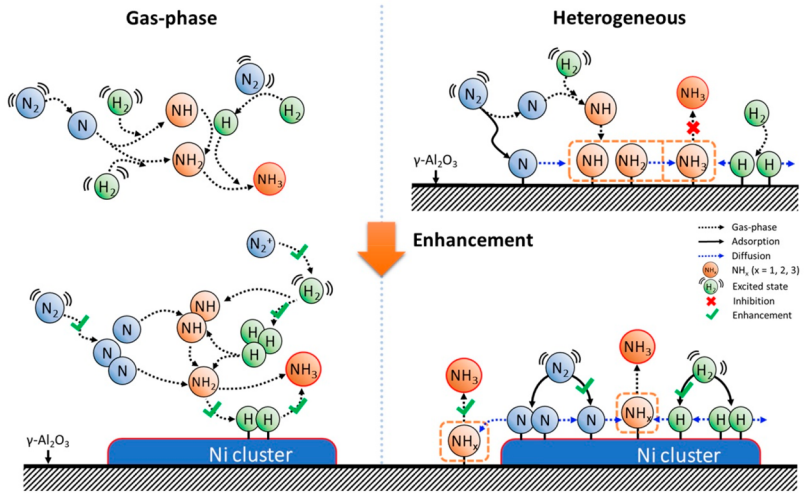

with decreasing M-N bond strength, which suggests that the improved yield with Ni/Al_2O_3 may have resulted from a lower rate of ammonia dissociation due to weaker M-N bonding. These results are in agreement with those obtained by Mehta et al., who also found that ammonia yields were improved with weaker nitrogen binding energies on the active metal sites.[13] By combining experiments with DFT microkinetic modeling, they determined that metals with a lower nitrogen binding strength have smaller hydrogenation barriers, which consequently leads to considerable rate enhancements. In agreement with this work, Ni/Al_2O_3 was identified as one of the best catalysts, while the performance of Fe/Al_2O_3 was relatively poor, indicating that the improved performance of Ni/Al_2O_3 over the other catalysts used in this work could be attributed to its smaller hydrogenation barriers.

It was proposed by Hong et al. that catalyst metal sites have a higher reaction coefficient for the dissociative adsorption of N_2 and H_2 (eqs S16−S19) than Al_2O_3,[61] and that the diffusion energy barrier (E_d) of L-H reactions (eqs S12−S15) on metal sites (0.2 eV) could be lower than that on Al_2O_3 surface sites (0.5 eV).[64] The inclusion of surface metal sites could, therefore, accelerate the diffusion of $N_2(s)$ and $H_2(s)$ and further promote the generation of $NH_x(s)$ species for ammonia synthesis. The more homogeneous dispersion of the transition metal particles on the surface of Ni/Al_2O_3 and Cu/Al_2O_3 (see HRTEM images, Figure 1) may have provided a more uniform dispersion of $N_2(s)$ and $H_2(s)$ across the catalyst surface, contributing to their improved performance compared with Fe/Al_2O_3. In addition to this, the Ni and Cu metal species were also smaller and had more uniform particle size distributions than the Fe species, and these properties have been reported to aid plasma-activated surface reactions.[65]

As shown in Figure 5, a comparison of the NH_3-TPD profiles for the fresh and spent Ni/Al_2O_3 catalysts indicated that more NH_3 desorbed from the spent catalyst at lower temperatures, signifying a reduction in the number of medium + strong acid sites. The change in acid sites may indicate that the interaction between the catalyst and the plasma during the reaction improved desorption of ammonia by altering the catalyst surface. As previously discussed, the easier NH_3 desorbs from the surface, the less likely it is to dissociate on the catalyst surface, which means these modifications likely improved the ammonia synthesis rate and yield.

Based on the results discussed in this work, a schematic diagram showing the possible mechanisms for ammonia synthesis by plasma-catalysis with Ni/Al_2O_3 is presented in Scheme 2. Ammonia synthesis by gas-phase reactions occurs through pathways that involve N, H, N_2, H_2, N_2*, H_2*, and NH_x (x = 1, 2) species (eqs R3, R14, R15, and R17−R22). In packing the discharge area with Al_2O_3 or M/Al_2O_3, the heterogeneous reactions become the dominant pathways (eqs S1−S19) and the ammonia yields are significantly improved. This phenomenon can be evidenced by the negligible effect of different metal catalysts (M/Al_2O_3) on the physical characteristics of the discharge in the plasma-catalytic synthesis of ammonia. In the presence of Ni/Al_2O_3, both gas-phase and heterogeneous reactions could be enhanced by significant alterations in the discharge, and through the adsorption, dissociation and surface reaction pathways provided by Ni. Ni/Al_2O_3 could produce more radicals (e.g., N, H, and NH) in the gas-phase by enhancing the reduced electric field and could also promote surface reactions by generating more NH_x through stepwise hydrogenation via the L-H mechanism

5. CONCLUSIONS

Plasma-enhanced synthesis of ammonia using transition metal catalysts (M/Al_2O_3, M= Fe, Ni, Cu) has been achieved at ambient pressure and near room temperature with a water-electrode DBD reactor. Compared to plasma synthesis of NH_3 without a catalyst, plasma-catalysis significantly enhanced the NH_3 synthesis rate and energy efficiency, which increased with different catalysts in the order: Ni/Al_2O_3 > Cu/Al_2O_3 > Fe/Al_2O_3 > Al_2O_3. All of the catalysts provided stable performances for at least 6 h, and Ni/Al_2O_3 maintained an efficient performance when recycled five times. The highest NH_3 synthesis rate of 471 μmol g^{-1} h^{-1} was achieved with Ni/Al_2O_3, which was 100% higher than that of plasma only. The performance was moderate compared to the state of the art. As there were no notable differences in the discharge characteristics for the three different metal catalysts, these results suggest that the catalytic effects provided by the chemistry of the catalyst surface are dominant over the physical effects of the catalysts in the plasma-catalytic synthesis of ammonia.

Most importantly, an insight into the synergetic effects of plasma-catalytic synthesis of ammonia at near-room temperature and atmospheric pressure has been investigated via a

DOI: 10.1021/acscatal.9b02538
ACS Catal. 2019, 9, 10780−10793

series of characterization methods. This indicates that the weak acid sites of the Al_2O_3 support can influence the performance of M/Al_2O_3 catalysts in the plasma-catalyzed synthesis of NH_3. Ni/Al_2O_3 produced a more uniform plasma discharge than Al_2O_3 or plasma only that enhanced both the gas-phase radical reactions of N, H and NH in the plasma and the reactions on the surface of the catalyst. The surface acidity of Ni/Al_2O_3 was also altered during the reaction, reducing the number of medium and strong acid sites, which may have also improved the rate of ammonia synthesis in situ. Furthermore, the synergy is also reflected in the order of the M-N bond strength (Ni-N < Cu-N < Fe-N); the weakest M-N bonds are expected to inhibit ammonia decomposition and enhance the turnover frequency for ammonia synthesis by reducing the energy required to dissociate ammonia from the metal sites on the catalyst surface.

■ ASSOCIATED CONTENT

Supporting Information

The Supporting Information is available free of charge on the ACS Publications website at DOI: 10.1021/acscatal.9b02538.

Experimental methods for OES and ICCD, turnover frequency (TOF) calculation, catalyst characterization (supplement), ICCD images of DBD packed with Ni/Al_2O_3 from two positions (1st and 2nd views), electrical characterization, calculation of mean electron density, calculated mean electron energy and electron energy distribution function (EEDF), energy efficiency of ammonia synthesis versus SEI, supplemental results of OES, and major reactions for plasma synthesis of ammonia (PDF)

■ AUTHOR INFORMATION

Corresponding Author

*E-mail: xin.tu@liverpool.ac.uk

ORCID

Jun Huang: 0000-0001-8704-605X

Xin Tu: 0000-0002-6376-0897

Notes

The authors declare no competing financial interest.

■ ACKNOWLEDGMENTS

Support of this work by the EPSRC Impact Acceleration Account (IAA) and Sydney Nano Grand Challenge is gratefully acknowledged.

■ REFERENCES

(1) Valera-Medina, A.; Xiao, H.; Owen-Jones, M.; David, W. I. F.; Bowen, P. J. Ammonia for Power. *Prog. Energy Combust. Sci.* **2018**, *69*, 63−102.

(2) Dunn, R.; Lovegrove, K.; Burgess, G. A Review of Ammonia-Based Thermochemical Energy Storage for Concentrating Solar Power. *Proc. IEEE* **2012**, *100*, 391−400.

(3) Chen, C.; Zhao, L.; Lavine, A. S. Feasibility of Using Ammonia-Based Thermochemical Energy Storage to Produce High-Temperature Steam or sCO_2. *Sol. Energy* **2018**, *176*, 638−647.

(4) Avery, W. H. A Role for Ammonia in the Hydrogen Economy. *Int. J. Hydrogen Energy* **1988**, *13*, 761−773.

(5) Morgan, E.; Manwell, J.; McGowan, J. Wind-Powered Ammonia Fuel Production for Remote Islands: A Case Study. *Renewable Energy* **2014**, *72*, 51−61.

(6) Yapicioglu, A.; Dincer, I. A Review on Clean Ammonia as a Potential Fuel for Power Generators. *Renewable Sustainable Energy Rev.* **2019**, *103*, 96−108.

(7) Tanabe, Y.; Nishibayashi, Y. Developing More Sustainable Processes for Ammonia Synthesis. *Coord. Chem. Rev.* **2013**, *257*, 2551−2564.

(8) Marnellos, G.; Stoukides, M. Ammonia Synthesis at Atmospheric Pressure. *Science* **1998**, *282*, 98−100.

(9) Brightling, J. Ammonia and the Fertiliser Industry: The Development of Ammonia at Billingham. *Johnson Matthey Technol. Rev.* **2018**, *62*, 32−47.

(10) *World Population Prospects: The 2017 Revision, Key Findings and Advance Tables*, 2017; p 161.

(11) *A Clean Planet for All A European Strategic Long-Term Vision for a Prosperous, Modern, Competitive and Climate Neutral Economy*; Brussels, 2018.

(12) Kitano, M.; Inoue, Y.; Yamazaki, Y.; Hayashi, F.; Kanbara, S.; Matsuishi, S.; Yokoyama, T.; Kim, S.-W.; Hara, M.; Hosono, H. Ammonia Synthesis Using a Stable Electride as an Electron Donor and Reversible Hydrogen Store. *Nat. Chem.* **2012**, *4*, 934.

(13) Mehta, P.; Barboun, P.; Herrera, F. A.; Kim, J.; Rumbach, P.; Go, D. B.; Hicks, J. C.; Schneider, W. F. Overcoming Ammonia Synthesis Scaling Relations with Plasma-Enabled Catalysis. *Nat. Catal.* **2018**, *1*, 269−275.

(14) Hong, J.; Prawer, S.; Murphy, A. B. Plasma Catalysis as an Alternative Route for Ammonia Production: Status, Mechanisms, and Prospects for Progress. *ACS Sustainable Chem. Eng.* **2018**, *6*, 15−31.

(15) Tu, X.; Verheyde, B.; Corthals, S.; Paulussen, S.; Sels, B. F. *Phys. Plasmas* **2011**, *18*, 080702.

(16) Tu, X.; Gallon, H. J.; Twigg, M. V.; Gorry, P. a; Whitehead, J. C. Dry Reforming of Methane over a Ni/Al_2O_3 Catalyst in a Coaxial Dielectric Barrier Discharge Reactor. *J. Phys. D: Appl. Phys.* **2011**, *44*, 274007.

(17) Tu, X.; Whitehead, J. C. Plasma-Catalytic Dry Reforming of Methane in an Atmospheric Dielectric Barrier Discharge: Understanding the Synergistic Effect at Low Temperature. *Appl. Catal., B* **2012**, *125*, 439−448.

(18) Xie, D.; Sun, Y.; Zhu, T.; Fan, X.; Hong, X.; Yang, W. Ammonia Synthesis and by-Product Formation from H_2O, H_2 and N_2 by Dielectric Barrier Discharge Combined with an Ru/Al_2O_3 Catalyst. *RSC Adv.* **2016**, *6*, 105338−105346.

(19) Hong, J.; Prawer, S.; Murphy, A. B. Production of Ammonia by Heterogeneous Catalysis in a Packed-Bed Dielectric-Barrier Discharge: Influence of Argon Addition and Voltage. *IEEE Trans. Plasma Sci.* **2014**, *42*, 2338−2339.

(20) Hong, J.; Aramesh, M.; Shimoni, O.; Seo, D. H.; Yick, S.; Greig, A.; Charles, C.; Prawer, S.; Murphy, A. B. Plasma Catalytic Synthesis of Ammonia Using Functionalized-Carbon Coatings in an Atmospheric-Pressure Non-Equilibrium Discharge. *Plasma Chem. Plasma Process.* **2016**, *36*, 917−940.

(21) Shah, J.; Wu, T.; Lucero, J.; Carreon, M. A.; Carreon, M. L. Nonthermal Plasma Synthesis of Ammonia over Ni-MOF-74. *ACS Sustainable Chem. Eng.* **2019**, *7*, 377−383.

(22) Bai, M.; Zhang, Z.; Bai, X.; Bai, M.; Ning, W. Plasma Synthesis of Ammonia With a Microgap Dielectric Barrier Discharge at Ambient Pressure. *IEEE Trans. Plasma Sci.* **2003**, *31*, 1285−1291.

(23) Shah, J.; Wang, W.; Bogaerts, A.; Carreon, M. L. Ammonia Synthesis by Radio Frequency Plasma Catalysis: Revealing the Underlying Mechanisms. *ACS Appl. Energy Mater.* **2018**, *1*, 4824−4839.

(24) Sugiyama, K.; Akazawa, K.; Oshima, M.; Miura, H.; Matsuda, T.; Nomura, O. Ammonia Synthesis by Means of Plasma over MgO Catalyst. *Plasma Chem. Plasma Process.* **1986**, *6*, 179−193.

(25) Bogaerts, A.; Neyts, E. C. Plasma Technology: An Emerging Technology for Energy Storage. *ACS Energy Lett.* **2018**, *3*, 1013−1027.

(26) Patil, B. S. Plasma (Catalyst) Assisted Nitrogen Fixation: Reactor Development for Nitric Oxide and Ammonia Production. *Ph.D. Thesis*, 2017.

(27) Mizushima, T.; Matsumoto, K.; Ohkita, H.; Kakuta, N. Catalytic Effects of Metal-Loaded Membrane-like Alumina Tubes on

Ammonia Synthesis in Atmospheric Pressure Plasma by Dielectric Barrier Discharge. *Plasma Chem. Plasma Process.* **2007**, *27*, 1−11.
(28) Akay, G.; Zhang, K. Process Intensification in Ammonia Synthesis Using Novel Coassembled Supported Microporous Catalysts Promoted by Nonthermal Plasma. *Ind. Eng. Chem. Res.* **2017**, *56*, 457−468.
(29) Neyts, E. C.; Ostrikov, K.; Sunkara, M. K.; Bogaerts, A. Plasma Catalysis: Synergistic Effects at the Nanoscale. *Chem. Rev.* **2015**, *115*, 13408−13446.
(30) Wang, L.; Yi, Y.; Wu, C.; Guo, H.; Tu, X. One-Step Reforming of CO_2 and CH_4 into High-Value Liquid Chemicals and Fuels at Room Temperature by Plasma-Driven Catalysis. *Angew. Chem., Int. Ed.* **2017**, *56*, 13679−13683.
(31) Wang, L.; Yi, Y.; Guo, H.; Tu, X. Atmospheric Pressure and Room Temperature Synthesis of Methanol through Plasma-Catalytic Hydrogenation of CO_2. *ACS Catal.* **2018**, *8*, 90−100.
(32) Stere, C. E.; Anderson, J. A.; Chansai, S.; Delgado, J. J.; Goguet, A.; Graham, W. G.; Hardacre, C.; Taylor, S. F. R.; Tu, X.; Wang, Z.; Yang, H. Non-Thermal Plasma Activation of Gold-Based Catalysts for Low-Temperature Water−Gas Shift Catalysis. *Angew. Chem., Int. Ed.* **2017**, *56*, 5579−5583.
(33) Whitehead, J. C. Plasma-Catalysis: Is It Just a Question of Scale? *Front. Chem. Sci. Eng.* **2019**, *13*, 264−273.
(34) Barboun, P.; Mehta, P.; Herrera, F. A.; Go, D. B.; Schneider, W. F.; Hicks, J. C. Distinguishing Plasma Contributions to Catalyst Performance in Plasma-Assisted Ammonia Synthesis. *ACS Sustainable Chem. Eng.* **2019**, *7*, 8621−8630.
(35) Mehta, P.; Barboun, P.; Go, D. B.; Hicks, J. C.; Schneider, W. F. Catalysis Enabled by Plasma Activation of Strong Chemical Bonds: A Review. *ACS Energy Lett.* **2019**, *4*, 1115−1133.
(36) Herrera, F. A.; Brown, G. H.; Barboun, P.; Turan, N.; Mehta, P.; Schneider, W. F.; Hicks, J. C.; Go, D. B. The Impact of Transition Metal Catalysts on Macroscopic Dielectric Barrier Discharge (DBD) Characteristics in an Ammonia Synthesis Plasma Catalysis Reactor. *J. Phys. D: Appl. Phys.* **2019**, *52*, 224002.
(37) Zi-Qing, W.; Yun-Cui, M.; Jian-Xin, L. Chemical Ruthenium Catalyst Supported on High-Surface-Area Basic ZrO_2 for Ammonia Synthesis. *Journal Mol. Catal. A, Chem.* **2013**, *378*, 307−313.
(38) Anderson, J. R. *Structure of Metallic Catalysts*, 1975.
(39) Wang, C.; Ma, X.; Ge, Q.; Xu, H. A Comparative Study of PdZSM-5, Pdβ, and PdY in Hybrid Catalysts for Syngas to Hydrocarbon Conversion. *Catal. Sci. Technol.* **2015**, *5*, 1847−1853.
(40) Iwamoto, M.; Akiyama, M.; Aihara, K.; Deguchi, T. Ammonia Synthesis on Wool-Like Au, Pt, Pd, Ag, or Cu Electrode Catalysts in Nonthermal Atmospheric-Pressure Plasma of N_2 and H_2. *ACS Catal.* **2017**, *7*, 6924−6929.
(41) Wang, Z.; Zhang, Y.; Neyts, E. C.; Cao, X.; Zhang, X.; Jang, B. W. L.; Liu, C. J. Catalyst Preparation with Plasmas: How Does It Work? *ACS Catal.* **2018**, *8*, 2093−2110.
(42) Liu, F.; Kong, W.; Qi, C.; Zhu, L.; Xiao, F. S. Design and Synthesis of Mesoporous Polymer-Based Solid Acid Catalysts with Excellent Hydrophobicity and Extraordinary Catalytic Activity. *ACS Catal.* **2012**, *2*, 565−572.
(43) Union, I.; Pure, O. F.; Chemistry, A. Reporting Physisorption Data for Gas/liquid Systems with Special Reference to the Determination of Surface Area and Porosity. *Pure Appl. Chem.* **1985**, *57*, 603−619.
(44) Meyer, E.; Moser, L.; De Temmerman, G.; Steiner, R.; Porosnicu, C.; Oberkofler, M.; Ben Yaala, M.; Marot, L.; Lungu, C. P. Quartz Micro-Balance and in Situ XPS Study of the Adsorption and Decomposition of Ammonia on Gold, Tungsten, Boron, Beryllium and Stainless Steel Surfaces. *Nucl. Fusion* **2018**, *58*, 106012.
(45) Lippitz, A.; Hübert, T. XPS Investigations of Chromium Nitride Thin Films. *Surf. Coat. Technol.* **2005**, *200*, 250−253.
(46) Ma, H.; Berthier, Y.; Marcus, P. AES, XPS, and TDS Study of the Adsorption and Desorption of NH_3 on Ultra-Thin Chromium Oxide Films Formed on Chromium Single Crystal Surfaces. *Appl. Surf. Sci.* **1999**, *153*, 40−46.
(47) Hagelaar, G. J. M.; Pitchford, L. C. Solving the Boltzmann Equation to Obtain Electron Transport Coefficients and Rate Coefficients for Fluid Models. *Plasma Sources Sci. Technol.* **2005**, *14*, 722−733.
(48) Gao, M.; Zhang, Y.; Wang, H.; Guo, B.; Zhang, Q.; Bogaerts, A. Mode Transition of Filaments in Packed-Bed Dielectric Barrier Discharges. *Catalysts* **2018**, *8*, 248.
(49) Tu, X.; Gallon, H. J.; Whitehead, J. C. *IEEE Trans. Plasma Sci.* **2011**, *39*, 2172−2173.
(50) Kim, H. H.; Kim, J. H.; Ogata, A. Microscopic Observation of Discharge Plasma on the Surface of Zeolites Supported Metal Nanoparticles. *J. Phys. D: Appl. Phys.* **2009**, *42*, 135210.
(51) Kim, H.-H.; Ogata, A. Nonthermal Plasma Activates Catalyst: From Current Understanding and Future Prospects. *Eur. Phys. J.: Appl. Phys.* **2011**, *55*, 13806.
(52) Mei, D.; Zhu, X.; He, Y.; Yan, J. D.; Tu, X. Plasma-Assisted Conversion of CO_2 in a Dielectric Barrier Discharge Reactor: Understanding the Effect of Packing Materials. *Plasma Sources Sci. Technol.* **2014**, *24*, 15011.
(53) Gomaa, M. M.; Gobara, H. M. Electrical Properties of Ni/silica Gel and Pt/γ-Alumina Catalysts in Relation to Metal Content in the Frequency Domain. *Mater. Chem. Phys.* **2009**, *113*, 790−796.
(54) Gadkari, S.; Gu, S. Influence of Catalyst Packing Configuration on the Discharge Characteristics of Dielectric Barrier Discharge Reactors: A Numerical Investigation. *Phys. Plasmas* **2018**, *25*, 63513.
(55) Van Laer, K.; Bogaerts, A. Fluid Modelling of a Packed Bed Dielectric Barrier Discharge Plasma Reactor. *Plasma Sources Sci. Technol.* **2015**, *25*, 15002.
(56) Kadowaki, Y.; Aika, K. I. Promoter Effect of Sm_2O_3 on Ru/Al_2O_3 in Ammonia Synthesis. *J. Catal.* **1996**, *161*, 178−185.
(57) Zhang, C.; Liu, Z.-P.; Hu, P. Stepwise Addition Reactions in Ammonia Synthesis: A First Principles Study. *J. Chem. Phys.* **2001**, *115*, 609−611.
(58) Park, Y. B.; Rhee, S. W. Bulk and Interface Properties of Low-Temperature Silicon Nitride Films Deposited by Remote Plasma Enhanced Chemical Vapor Deposition. *J. Mater. Sci.: Mater. Electron.* **2001**, *12*, 515−522.
(59) Bayram, S. B.; Freamat, M. V. *Vibrational Spectra of N_2: An Advanced Undergraduate Laboratory*, 2015; Vol. *664*, pp 663−669.
(60) Gómez-Ramrez, A.; Cotrino, J.; Lambert, R. M.; González-Elipe, A. R. Efficient Synthesis of Ammonia from N_2 and H_2 alone in a Ferroelectric Packed-Bed DBD Reactor. *Plasma Sources Sci. Technol.* **2015**, *24*, 65011.
(61) Hong, J.; Pancheshnyi, S.; Tam, E.; Lowke, J. J.; Prawer, S.; Murphy, A. B. Corrigendum: Kinetic Modelling of NH_3 Production in N_2 − H_2 Non-Equilibrium Atmospheric-Pressure Plasma Catalysis. *J. Phys. D: Appl. Phys.* **2017**, *50*, 154005.
(62) Uyama, H.; Matsumoto, O. Synthesis of Ammonia in High-Frequency Discharges. *Plasma Chem. Plasma Process.* **1989**, *9*, 13−24.
(63) Wang, L.; Yi, Y.; Zhao, Y.; Zhang, R.; Zhang, J.; Guo, H. NH_3 Decomposition for H_2 Generation: Effects of Cheap Metals and Supports on Plasma - Catalyst Synergy. *ACS Catal.* **2015**, *5*, 4167−4174.
(64) Carrasco, E.; Jimenez-Redonado, M.; Tanarro, I.; Herrero, V. J. Neutral and Ion Chemistry in Low Pressure Dc Plasmas of H_2/N_2 Mixtures: Routes for the Efficient Production of NH_3 and NH_4^+. *Phys. Chem. Chem. Phys.* **2011**, *13*, 19561−19572.
(65) Zeng, Y.; Zhu, X.; Mei, D.; Ashford, B.; Tu, X. Plasma-Catalytic Dry Reforming of Methane over γ-Al_2O_3 supported Metal Catalysts. *Catal. Today* **2015**, *256*, 80−87.

DOI: 10.1021/acscatal.9b02538
ACS Catal. 2019, 9, 10780−10793